

# Frozonium: Freezing Anharmonicity in Floquet Superconducting Circuits

Keiran Lewellen,<sup>1</sup> Rohit Mukherjee,<sup>1,\*</sup> Haoyu Guo,<sup>1,\*</sup> Saswata Roy,<sup>1</sup> Valla Fatemi,<sup>2</sup> and Debanjan Chowdhury<sup>1,†</sup>

<sup>1</sup>*Department of Physics, Cornell University, Ithaca NY 14853.*

<sup>2</sup>*School of Applied and Engineering Physics, Cornell University, Ithaca NY 14853.*

Floquet engineering is a powerful method that can be used to modify the properties of interacting many-body Hamiltonians via the application of periodic time-dependent drives. Here we consider the physics of an inductively shunted superconducting Josephson junction in the presence of Floquet drives in the fluxonium regime and beyond, which we dub the *frozonium* artificial atom. We find that in the vicinity of special ratios of the drive amplitude and frequency, the many-body dynamics can be tuned to that of an effectively linear bosonic oscillator, with additional nonlinear corrections that are suppressed in higher powers of the drive frequency. By analyzing the inverse participation ratios between the time-evolved frozonium wavefunctions and the eigenbasis of a linear oscillator, we demonstrate the ability to achieve a novel dynamical control using a combination of numerical exact diagonalization and Floquet-Magnus expansion. We discuss the physics of *resonances* between quasi-energy states induced by the drive, and ways to mitigate their effects. We also highlight the enhanced protection of frozonium against external sources of noise present in experimental setups. This work lays the foundation for future applications in quantum memory and bosonic quantum control using superconducting circuits.

## I. Introduction

The past two decades have seen a series of remarkable breakthroughs in the field of circuit quantum electrodynamics [1–3] — the microwave-frequency quantum light-matter interactions between harmonic oscillators and superconducting artificial atoms. At present, multiple commercially available quantum computing hardware platforms are based on superconducting qubits [4–6], which leverage capacitively shunted and coupled Josephson junctions to create artificial atoms with individually-addressable quantum transitions [2]. Through the manipulation and control of the occupation of these levels via microwave-frequency driving, quantum information can be processed to accomplish a variety of non-trivial tasks.

In the *transmon* regime of capacitively coupled Josephson junctions, which has been of great practical significance in recent times, theoretical work on the undriven array has pointed out the susceptibility of the coupled system towards chaos [7–12], which can become detrimental towards scaling up the devices in the future. At present, susceptibility to chaos is mitigated by the use of tunable couplers [13] or via frequency detuning [14]. Both of these approaches introduce design and circuit complexity, potentially introducing new sources of decoherence; the viability of scalability to thousands of qubits remains presently unclear. Alternative methods of addressing this susceptibility to chaos or decoherence in general are thus of significant interest, and the use of Floquet drives or Floquet analysis is an active area of study to this end [15–24].

To be concrete, consider the following driven transmon

Hamiltonian,

$$\mathcal{H}(t) = H_{\text{transmon}} + f(t)H_{\text{drive};\hat{n}}, \quad (1a)$$

$$H_{\text{transmon}} = -E_J \cos(\hat{\varphi}) + 4E_c(\hat{n} - n_g)^2, \quad (1b)$$

$$H_{\text{drive};\hat{n}} = \hat{n}, \quad (1c)$$

where  $\hat{n}$  is the Cooper pair number operator,  $\hat{\varphi}$  is the superconducting phase satisfying the usual commutation relation  $[\hat{\varphi}, \hat{n}] = i$ , and  $n_g$  is the charge offset resulting from the compactness of  $\hat{\varphi}$  in the range  $(-\pi, \pi)$  [25].  $E_c$  is the capacitive charging energy and  $E_J$  represents the Josephson energy; see Fig. 1a. The Floquet drive,  $f(t)$ , has an amplitude,  $A$ , and period  $T$ , such that  $f(t) = f(t + T)$  (i.e. with fundamental drive frequency,  $\omega = 2\pi/T$ ). Previous work by some of us [26] showed that there exist special *freezing points* at fixed ratios of  $A/\omega$  under the Floquet drive, where the periodic  $\cos(\hat{\varphi})$  term is suppressed. In the limit  $\omega \rightarrow \infty$ , the Hamiltonian is reduced to consisting of just the charge variable, which thereby exhibits no quantum dynamics. For a finite  $\omega$ , the induced nonlinearities were suppressed as  $\mathcal{O}(1/\omega)$ , resulting in a significant reduction in the growth of chaos in coupled transmon systems.

Importantly, the offset charge was not considered in that work, and, even in the limit of a large  $\omega$ , previous studies suggest it will result in a strong dephasing of the charge degree of freedom due to well-documented charge noise [2, 27–30]. We will analyze this intuitive expectation quantitatively for the parametric dependence on static offset charge. Nonetheless, realizations of superconducting quantum circuits which afford complete insensitivity to charge noise and other sources of decoherence are highly desirable [31]. With this in mind, the main focus of the present manuscript is on a modified superconducting circuit with an inductive shunt, which we will find leads to a number of important benefits.

Our central novel result for the freezing points associated with the inductively shunted superconducting cir-

\* These authors contributed equally to this work

† debanjanchowdhury@cornell.edu

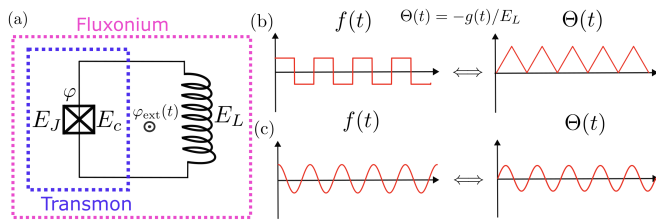


FIG. 1: (a) Schematic illustration of a transmon circuit consisting of a Josephson junction and capacitor (enclosed by blue dashed line), and a fluxonium circuit with an inductive shunt (enclosed by magenta dashed line). The (b) square-wave, and (c) cosine-wave Floquet drive,  $f(t)$ , in Eq. (2a) controls the (b) triangle-wave, and (c) sine-wave Floquet drives,  $\Theta(t) = \int_0^t dt' f(t')$ , respectively; see Eq. (5).

cuits will be their non-chaotic *quantum* dynamics, which we dub as “frozonium”. Specifically, at the freezing point that is induced by a flux drive, the circuit is well-approximated as a harmonic oscillator at the leading order in  $\mathcal{O}(1/\omega)$ . Therefore, the drives can interpolate the circuit between harmonic and strongly anharmonic configurations. Furthermore, the inductive shunt removes the offset charge, and, although these circuits admit an external flux which can be noisy, we show that the freezing points exhibit a largely flux-insensitive spectrum. Therefore, the frozonium can be utilized to increase robustness to external sources of noise, while additionally serving as a novel platform for both qubit and bosonic formulations of quantum information processing.

Let us add an inductive shunt to the model of Eq. (1a),

$$\mathcal{H}(t) = H_{\text{fluxonium}} + f(t)H_{\text{drive};\hat{n}} + g(t)H_{\text{drive};\hat{\varphi}}, \quad (2a)$$

$$H_{\text{fluxonium}} = H_{\text{transmon}} + \frac{E_L}{2}\hat{\varphi}^2, \quad (2b)$$

$$H_{\text{drive};\hat{\varphi}} = \hat{\varphi}, \quad (2c)$$

where the additional terms associated with  $E_L$  are due to the inductive energies, and we will find the second drive,  $g(t)$ , is necessary to extend the freezing phenomenology to this setting; see Fig. 1a. Note that  $H_{\text{transmon}}$  no longer has the offset charge parameter in the presence of the inductive shunt. We leave the precise relationship between  $f(t)$  and  $g(t)$  unspecified for now, but as we show in Sec. II, for a specific choice of drives they are effectively equivalent to a flux drive. Note that while we will continue to refer to the above circuit as “fluxonium”, the phenomenology we discuss below is not restricted to any specific hierarchy of energy scales among  $E_L$ ,  $E_J$  and  $E_C$  [32]. The new inductive term  $\hat{\varphi}^2$  leads to two key differences of both practical and theoretical significance.

First, we will find that the effective Hamiltonian at freezing for the driven fluxonium is always quantum mechanical, even in the  $\omega \rightarrow \infty$  limit. In that limit, the Hamiltonian is further both quantum mechanical and fully non-chaotic, unlike all previous examples of dy-

namical freezing [26, 33–38]. Perturbing away from the  $\omega \rightarrow \infty$  limit down to realistic frequencies introduces additional quantum mechanical structure that has interesting implications for control of the residual nonlinearities.

Second, the inductive shunt breaks the periodicity in  $\hat{\varphi}$  of the Hamiltonian, effectively eliminating the static offset charge  $n_g$  present in the conventional transmon [32, 39]. Instead the formation of a closed loop in the circuit encompassing the inductive and Josephson elements results in flux noise through this loop being the primary source of decoherence. Time-dependent fluctuations in this flux lead to a time dependence in the difference between the energies of the circuit. In particular, random variations in the energy difference between the computational states,  $|\epsilon_1 - \epsilon_0|$  results in phase errors — the build up of an unknown phase between the computational states. The flux noise spectrum tends to be slow relative to the energy scales of the system [30, 40–44]. As we will demonstrate below, the driven fluxonium at freezing is significantly less sensitive to flux noise than the static circuit.

The remainder of this manuscript is organized as follows. In Sec. IIA we review the basics of Floquet-Magnus expansion as applied to the driven fluxonium circuit, which serves as a useful starting point for interpreting our numerical results. In Sec. IIB we present the numerical results obtained using exact diagonalization (ED) for a single driven fluxonium. In Sec. IIC we demonstrate the robustness against well known sources of charge and flux noise in the driven transmon and fluxonium near freezing. We end in Sec. III with an outlook towards open problems and possible applications. The appendices contain additional technical details.

## II. Results

### A. Floquet-Magnus Expansion

To begin with, we describe the general intuition for the expected results by performing a Floquet-Magnus expansion; see Appendix A for additional details. Moreover, this will also help clarify the required relationship between the two drive functions,  $f(t)$  and  $g(t)$ , that can enable the novel control of the induced nonlinearities. In order to obtain the quasi-energy spectrum and late-time behavior associated with the model in Eq. (2a), we first perform a time-dependent unitary transformation to a co-moving reference frame,  $W(t) = e^{-i\Theta(t)H_{\text{drive};\hat{n}}}$ , where  $\Theta(t) = \int_0^t dt' f(t')$ . The transformed Hamiltonian is then,

$$\mathcal{H}_{\text{mov}}(t) = W^\dagger(t)[\mathcal{H}(t) - \partial_t]W(t) \quad (3a)$$

$$= W^\dagger(t)[H_{\text{fluxonium}} + g(t)H_{\text{drive};\hat{\varphi}}]W(t) \quad (3b)$$

This can be simplified further using the Baker-Campbell-Hausdorff (BCH) formula to yield,

$$\begin{aligned} \mathcal{H}_{\text{mov}}(t) &= H_{\text{transmon}}[\hat{n}, \hat{\varphi} - \Theta(t)] + \frac{E_L}{2} \hat{\varphi}^2 \\ &+ \Theta(t) E_L \hat{\varphi} + g(t) \hat{\varphi}. \end{aligned} \quad (4)$$

If we now choose a specific relationship between the drives such that  $g(t) = -E_L \Theta(t)$ , the last two terms above cancel mutually, and we arrive at the significantly simplified Hamiltonian,

$$\mathcal{H}_{\text{mov}}(t) = H_{\text{transmon}}[\hat{n}, \hat{\varphi} - \Theta(t)] + \frac{E_L}{2} \hat{\varphi}^2. \quad (5)$$

Allowing for the presence of an external flux,  $\varphi_{\text{ext}}$ , through the inductive-Josephson loop gives,

$$\mathcal{H}_{\text{mov}}(t) = H_{\text{quad}} - E_J \cos(\hat{\varphi} + \varphi_{\text{ext}} - \Theta(t)), \quad (6a)$$

$$H_{\text{quad}} = 4E_c \hat{n}^2 + \frac{E_L}{2} \hat{\varphi}^2. \quad (6b)$$

When making reference to any analytical discussions of the problem, this is the Hamiltonian we work with in the remainder of the manuscript. For the driven fluxonium, it is useful to note that the Hamiltonian in Eq. (6a) can also be realized directly via an external microwave flux drive,  $\Theta(t)$ , without the need for driving both  $\hat{n}$  and  $\hat{\varphi}$ . This provides an alternative experimental route for achieving dynamical control. Unless otherwise stated, we fix the static flux  $\varphi_{\text{ext}} = \pi$  in the remainder of the manuscript.

For the remainder of this manuscript, we consider two forms of the periodic Floquet drive,  $\Theta(t)$ : the triangle-wave drive and the sine-wave drive; see Fig. 1b,c. Specifically,

$$\Theta_{\text{tw}}(t) = \alpha \cdot 2\pi \left\lfloor \frac{\omega}{2\pi} t - \left\lfloor \frac{\omega}{2\pi} t + \frac{1}{2} \right\rfloor \right\rfloor, \quad (7a)$$

$$\Theta_{\text{sin}}(t) = \alpha \sin(\omega t), \quad (7b)$$

where  $\lfloor \cdot \rfloor$  indicates taking the integer part of a real number (see Fig. 1c),  $\alpha$  is the phase amplitude of the drive, and  $\omega$  its frequency which we will take to be in the gigahertz (GHz) range. (Note that while  $\Theta_{\text{tw}}(t)$  has a net DC offset, this is notational, and the offset can be absorbed into the definition of  $\varphi_{\text{ext}}$ .) If the Hamiltonian in Eq. (6a) is achieved directly via an external flux drive, then the form of the drive is simply given by  $\Theta(t)$  in each case. If the Hamiltonian in Eq. (6a) is achieved via driving both  $\hat{n}$  and  $\hat{\varphi}$ , then the drives are given by

$$f_{\text{tw}}(t) = A \operatorname{sgn}[\sin(\omega t)], \quad g_{\text{tw}}(t) = -E_L \Theta_{\text{tw}}(t), \quad (8a)$$

$$f_{\text{sin}}(t) = A \cos(\omega t), \quad g_{\text{sin}}(t) = -E_L \Theta_{\text{sin}}(t), \quad (8b)$$

where  $A$  is the amplitude of the  $\hat{n}$  drive, and  $\alpha = A/\omega$ , respectively. We focus primarily on results for the triangle-wave drive in the main text, and leave a discussion of the results for the sine drive for Appendix C. Furthermore,

unless otherwise noted, we will work with  $E_c/h = 0.33$  GHz,  $E_L/h = 1$  GHz, and  $E_J/h = 4$  GHz [45].

Starting with the Hamiltonian in Eq. (6a), the leading order term of the Magnus expansion is given by,

$$\mathcal{H}_{\text{eff}}^0 = \frac{1}{T} \int_0^T dt \mathcal{H}_{\text{mov}}(t), \quad (9)$$

where depending on the form of the periodic drive, we obtain,

$$\mathcal{H}_{\text{eff;tw}}^0 = H_{\text{quad}} - \frac{E_J}{\pi\alpha} (\sin(\hat{\varphi}) + \sin(\pi\alpha - \hat{\varphi})) + \dots, \quad (10a)$$

$$\mathcal{H}_{\text{eff;sin}}^0 = H_{\text{quad}} - E_J J_0(\alpha) \cos(\hat{\varphi}) + \dots. \quad (10b)$$

Here  $J_0(\dots)$  is the Bessel function of first kind, and the  $\dots$  represent corrections suppressed in  $O(1/\omega)$ . Thus, the leading order nonlinearity vanishes at certain fixed parameter values:

$$\alpha \approx 2n, \quad n \in \mathbb{Z} \quad (\text{Triangle wave}) \quad (11a)$$

$$\alpha \approx \text{zeros of } J_0(\dots) \quad (\text{Sine wave}). \quad (11b)$$

As a result, the effective Hamiltonian for the driven fluxonium represents a linear *quantum* harmonic oscillator given by Eq. (6b), with all of the higher-order nonlinearities suppressed in  $O(1/\omega)$ . As noted previously, this is distinct from *all* previous discussions of dynamical freezing (including the driven transmons [26]), where the effective Hamiltonian in the  $\omega \rightarrow \infty$  limit is purely classical. Therefore, this relatively straightforward analysis already suggests that by varying both  $\alpha$  and  $\omega$ , we can tune the relative strength of nonlinearity associated with the dynamics of the effective Hamiltonian in the vicinity of the freezing points. Next we will turn to a direct numerical analysis of the driven fluxonium.

## B. Numerical Exact Diagonalization

Let us now simulate numerically the system of a single fluxonium driven with a triangle-wave drive,  $\Theta(t)$ ; see Appendix B for technical details. Based on our discussion in Sec. II A, we expect the effective Hamiltonian near freezing (see Eq. (11a)) to be well described by the quadratic Hamiltonian in Eq. (6b). Our goal is to diagnose the extent to which the numerically exact eigenstates for the full driven fluxonium overlap with the eigenstates of the harmonic oscillator described by  $H_{\text{quad}}$  in Eq. (6b). To quantify this, we first choose an eigenstate of  $H_{\text{quad}}$  as the initial state, and time-evolve it with the driven Hamiltonian,  $\mathcal{H}_{\text{mov}}(t)$  in Eq. (6a) for  $N_F$  Floquet cycles. We compute the inverse participation ratio (IPR) at the end of the time evolution, which is defined

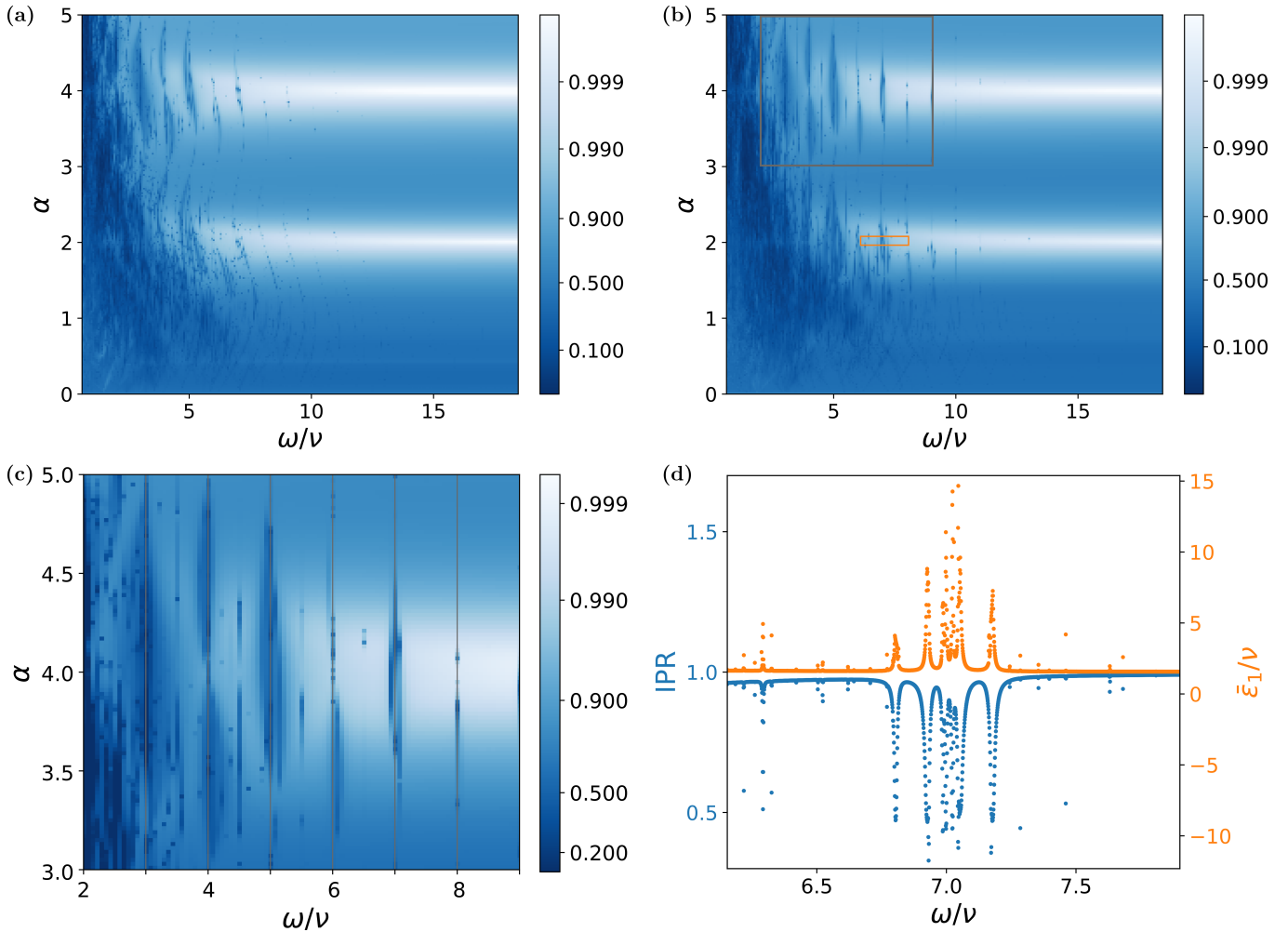


FIG. 2: The IPR (Eq. (12a)) as a function of  $\alpha$  and  $\omega/\nu$  for a fluxonium driven via  $\Theta_{\text{tw}}(t)$  (Eq. (7a)) with  $\varphi_{\text{ext}} = \pi$  time-averaged over  $N_F = 10,000$  cycles. Here  $\nu$  is the fundamental frequency (given in Eq. 13) of the oscillator defined in Eq. (6b).  $|\Psi(0)\rangle$  is initialized to the (a) ground state, and (b) first excited state of  $H_{\text{quad}}$  in Eq. (6b). The white horizontal bands with  $\text{IPR} > 0.99$  centered around  $\alpha = 2, 4$  are associated with freezing region (see Eq. (11a)). (c) Zoom-in from panel (b) [grey rectangle] showing vertical streaks of  $\text{IPR} \ll 1$  embedded in a region with  $\text{IPR} \approx 1$ . The color-scale in (a)-(c) is chosen to have an arctanh form, normalized to a domain,  $(1/d_H, 1)$ , with  $d_H = 70$ . We adopt the Hamiltonian parameters  $E_c/h = 0.33$  GHz,  $E_L/h = 1$  GHz, and  $E_J/h = 4$  GHz, motivated by Ref. [45] (d) IPR at fixed  $\alpha$  as a function of  $\omega/\nu$  (blue curve) from panel (b) [orange rectangle]. The frequencies with a drop in IPR correlate with peaks in  $\bar{\epsilon}_k$  for the first excited state defined in Eq. (14a).

as

$$\text{IPR} = \sum_{i=1}^{d_H} |\langle \Phi_i | \Psi(t) \rangle|^4, \text{ where} \quad (12a)$$

$$|\Psi(t)\rangle = \mathcal{T} \exp\left(-\int_0^t dt' i\mathcal{H}_{\text{mov}}(t')\right) |\Psi(0)\rangle, \quad (12b)$$

and  $\mathcal{T}$  denotes time-ordering. Here  $\{|\Phi_i\rangle\}$  represents a complete eigenbasis associated with the quantum harmonic oscillator in Eq. (6b). Note that while the local Hilbert-space is formally unbounded, for our numerical computations we truncate to a relatively large low-energy subspace with  $d_H = 70$ . For evaluating the IPR, we choose  $N_F = 10,000$  cycles.

At time  $t = 0$ , the IPR starts out with a value of 1. For a given value of  $\alpha$  and  $\omega$ , if the effective Hamiltonian

for the driven system is well approximated by  $H_{\text{quad}}$ , we expect  $\text{IPR} \approx 1$ . On the other hand, if the system “equilibrates” to a featureless “infinite-temperature” state as a result of the time-evolution under the full nonlinear theory, we expect  $\text{IPR} \sim O(1/d_H)$ , where  $d_H$  is the Hilbert space dimension. Generically, away from the freezing points, the IPR will assume a value that is different from these two limiting cases. The actual value is a function of the drive frequency, proximity to freezing, and  $N_F$ . This indicates that the effective Hamiltonian is not well approximated by  $H_{\text{quad}}$ , and the inevitable approach to thermalization is then controlled by pre-thermal physics. Importantly, even the freezing points can eventually thermalize depending on the driving protocol [46], but the associated timescales can be exponentially long in the

drive-frequency, and therefore not of any practical concern.

In Fig. 2 we analyze the stroboscopically averaged IPR over  $N_F (= 10,000)$  Floquet cycles as a function of  $\alpha$  and  $\omega/\nu$ . Here  $\nu$  is the fundamental energy of the oscillator described by  $H_{\text{quad}}$  given by

$$\nu/h = \sqrt{8E_C E_L}/h \approx 1.63 \text{ GHz}. \quad (13)$$

We initialize  $|\Psi(0)\rangle$  to the ground state (Fig. 2 (a)) and the first excited state (Fig. 2 (b)) of  $H_{\text{quad}}$  respectively. As expected from Eq. (11a), we find clear evidence of horizontal “bands” (white regions in Figs. 2a, b) centered around  $\alpha = 2, 4, \dots$  where the IPR  $\gtrsim 0.99$ . Furthermore, the IPR is closer to 1 above a threshold frequency set by the intrinsic single-particle energy scales, as noted previously in the context of freezing in Ref. [26]. We have also noticed that the width of the vertical region at low  $\omega$  with a small IPR increases for  $|\Psi(0)\rangle$  with higher energy. In order to recover an IPR  $\rightarrow 1$  for such states, the drive frequency needs to be correspondingly larger.

Let us now turn to one of the most striking features of our results in Fig. 2a, b, associated with the narrow vertical “streaks” with a suppressed value of IPR  $\ll 1$  embedded in a region near freezing with IPR  $\rightarrow 1$ . In Fig. 2c, we show a zoomed-in region of the data in Fig. 2b centered around  $\alpha = 4$  that shows these streaks clearly. As we shall now discuss, these regions are associated with pairs of states whose quasi-energies differ exactly by the drive frequency  $\omega$ , resulting in a *resonance* phenomenon. At resonance, the pair of states are strongly hybridized due to the Floquet drive, resulting in spike-like features in the Floquet quasi-energies. To demonstrate the correlation between IPR drop and spike features of quasi-energies, let us now introduce a period-averaged Floquet quasi-energy over  $0 \leq t \leq T$  [47, 48],

$$\bar{\varepsilon}_k = \frac{1}{T} \int_0^T dt \langle \phi_k(t) | \mathcal{H}_{\text{mov}}(t) | \phi_k(t) \rangle, \quad (14a)$$

$$|\phi_k(t)\rangle = \mathcal{T} \exp \left( - \int_0^t dt' i \mathcal{H}_{\text{mov}}(t') \right) |\phi_k(0)\rangle \quad (14b)$$

Here  $|\phi_k(t)\rangle$  are the Floquet eigenstates of  $H_{\text{mov}}(t)$ , with  $|\phi_k(T)\rangle = |\phi_k(0)\rangle$ . Note that  $\bar{\varepsilon}_k$  as defined above, is not folded modulo  $\omega$  and it serves as a proxy for studying the spectrum of the Floquet Hamiltonian. By analyzing the IPR at a fixed  $\alpha$  as a function of  $\omega$  (see orange rectangle in Fig. 2b), we find that the precipitous drop away from IPR  $\approx 1$  coincides with strong peaks in  $\bar{\varepsilon}_k$ ; see Fig. 2d. Relatedly when IPR  $\approx 1$  away from the streak-like regions,  $\bar{\varepsilon}_k$  remains featureless.

To better characterize the origin of the resonances introduced above, we plot the five lowest period averaged quasi-energies (blue dots) for the driven fluxonium in Fig. 3 as a function of  $\alpha$ , and for three different values of increasing  $\omega$ . The  $|\phi_k(t)\rangle$  in Eq. 14a used to evaluate these are obtained from the numerical exact diagonalization. In the figure, we also show  $\bar{\varepsilon}_k^{\text{FM}}$  (orange dashed

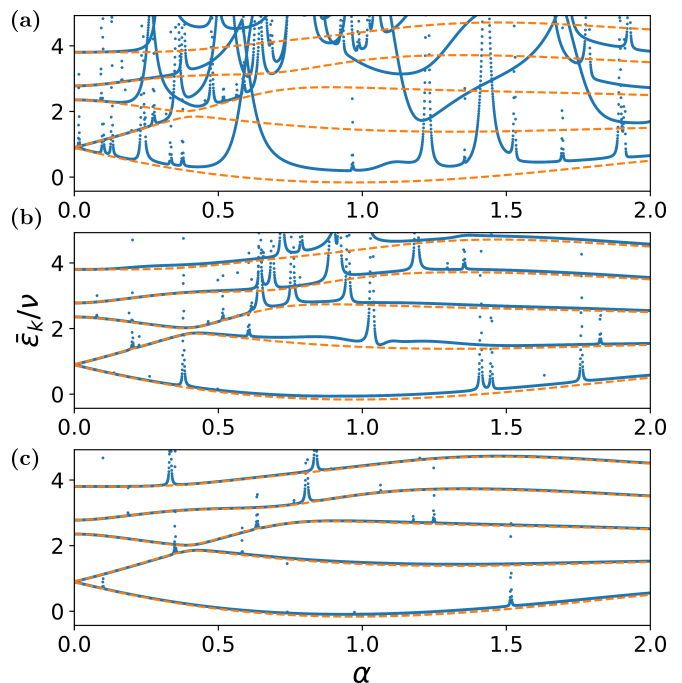


FIG. 3: The period averaged quasi-energies,  $\bar{\varepsilon}_k$  (Eq. (14a)) as a function of  $\alpha$  for a driven fluxonium at (a)  $\omega/\nu = 6.15$ , (b)  $\omega/\nu = 9.23$ , and (c)  $\omega/\nu = 12.31$ , respectively. The result is normalized by the fluxonium oscillator energy  $\nu$  (Eq. (13)). All other parameters are as in Fig. 2. Blue data points are obtained from numerical exact diagonalization. Orange dashed lines are obtained using the zeroth-order Floquet-Magnus expansion (Eq. (10a)).

line) for the same five levels based on the zeroth-order Floquet-Magnus expansion (Eq. (10a)). As expected, we find better agreement between the two sets of results with increasing drive frequency. Additionally, the number of resonances and the associated singular features in  $\bar{\varepsilon}_k$  decrease with increasing frequency. With increasing frequency, we also notice that the quasi-energy level-spacing interpolates more smoothly between the anharmonic regime ( $\alpha = 0$ ) to the harmonic regime near freezing ( $\alpha = 2$ ).

Thus far we have not shown the exact pairs of quasi-energy levels that control these resonances. To track these down, in Fig. 4 we have plotted the lowest twenty period averaged quasi-energies along with the predictions of the zeroth-order Floquet-Magnus expansion for the drive frequency in Fig. 3c. We have scanned for all pairs of period-averaged quasi-energies  $\bar{\varepsilon}_i^{\text{FM}}$  obtained from the zeroth-order Floquet-Magnus where  $|\bar{\varepsilon}_i^{\text{FM}} - \bar{\varepsilon}_j^{\text{FM}}| \in (\omega - \Delta\omega, \omega + \Delta\omega)$  (with  $\Delta\omega = 0.03\nu \ll \omega$ ) as a function of  $\alpha$ . We have marked these pairs of quasi-energy levels [as (A), (B) and with colored bars] in Fig. 4. At these values of  $\alpha$ , we expect a strong hybridization between Floquet eigenstates due to resonances. These resonances are between states separated by  $\omega$  in  $\bar{\varepsilon}_k$ , and are known to be related to heating of the driven system [49]. We find a one-to-one correspondence between the

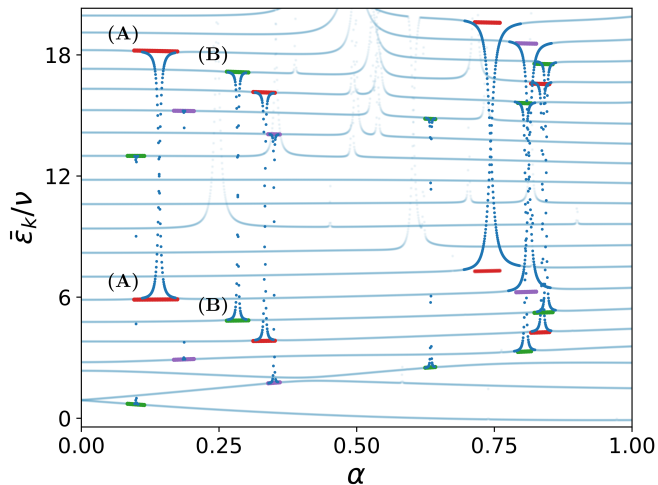


FIG. 4: The period averaged quasi-energies,  $\bar{\epsilon}_k$ , as a function of  $\alpha$  for a driven fluxonium at  $\omega/\nu = 12.31$ . The result is normalized by the fluxonium oscillator energy  $\nu$  (Eq. (13)). All other parameters are as in Fig. 2. The locations for the resonances determined from the numerically evaluated averaged quasi-energies (blue) agree well with those obtained from the zeroth order Floquet-Magnus results, which are marked by pairs of red, green, and purple bars. The latter is obtained using the period-averaged quasi-energy  $\bar{\epsilon}_i^{\text{FM}}$  from the Floquet Magnus expansion and the condition  $|\bar{\epsilon}_i^{\text{FM}} - \bar{\epsilon}_j^{\text{FM}}| \in (\omega - \Delta\omega, \omega + \Delta\omega)$ , where  $\omega = 12.31\nu$  and we choose a small  $\Delta\omega = 0.03\nu$ . As an example, we mark two such pairs of states as (A) and (B). Note that the resonances are only plotted for partners that lie within the twenty quasi-energies.

resonances in the period averaged Floquet quasi-energies obtained from the zeroth-order Floquet-Magnus expansion and the direct numerical results. To summarize, the Floquet-Magnus expansion can provide a good approximation for the smooth features of the period-averaged Floquet quasi-energies, but fails to capture the spike-like features associated with resonances. However, the location of the resonances can still be approximately determined from the Floquet-Magnus result.

An important limiting case of these resonances occurs near freezing points where the effective Hamiltonian for the driven fluxonium is well approximated by  $H_{\text{quad}}$ . At these points the energy level-spacing between the eigenstates becomes approximately uniform and is given by  $\nu$  (see Eq. 13). Strong resonances are thus expected to occur for drive frequencies satisfying  $\omega/\nu \in \mathbb{Z}$ . These resonances can be seen clearly in Fig. 2c in which we plot the stroboscopically averaged IPR (w.r.t. first excited state of  $H_{\text{quad}}$ ) of a single driven fluxonium near freezing as a function of  $\alpha$  and  $\omega/\nu$ . At integer values of  $\omega/\nu$ , we observe the sharp decreases in IPR indicative of resonances. Additionally, weaker resonances are marked by the suppression in IPR at the half-integer ratios of  $\omega/\nu$ . At these points, there exist eigenenergies separated by a gap of approximately  $2\omega$ , resulting in the observation of additional resonances. It is worth pointing out that for

the sine-wave drive at freezing, the leading nonlinear correction to the effective Hamiltonian beyond  $H_{\text{quad}}$  scales as  $\sim \hat{n} \cos \hat{\varphi}/\omega$ . By choosing  $|\Psi(0)\rangle$  to be an eigenstate of this nonlinear oscillator, we find an increase in the magnitude of the IPR compared to an eigenstate of  $H_{\text{quad}}$ ; see Appendix C.

### C. Robustness to Variations in External Flux

We now return to one of the main practical advantages of the Floquet protocol in the vicinity of freezing, namely of an enhanced robustness to external noise. Before describing the results for the driven fluxonium due to variations in the external flux,  $\varphi_{\text{ext}}$ , let us briefly comment on the results for the driven transmon [Eq. (1b)] in the presence of variations in  $n_g$ . Static transmons are known to be resistant to fluctuations in charge noise since the large Josephson energy (relative to charging energy) exponentially suppresses the charge dispersion of the low-lying eigenstates [27]. On the other hand, driven transmons at generic values of the drive amplitude become dramatically more susceptible to effects of charge noise [2, 28]. At freezing points, the driven transmons behave as a pure charging island, which have quadratic dependence on offset charge. Within the Floquet-Magnus expansion, this can be understood as follows. The term in the effective Hamiltonian stemming from the external charge noise is of the form  $(n_g \hat{n})$ , which commutes with the zeroth-order term  $(4E_c \hat{n}^2)$ . The spectrum of the dynamically frozen transmon is then governed by the higher order corrections. To demonstrate this numerically, instead of analyzing the effects of a fully time-dependent noise  $n_g(t)$ , we assume that variations in charge noise occur on a slower timescale compared to the relevant energy scales of our driven system [30, 50]. Within this adiabatic approximation, we treat  $n_g$  as a quenched variable.

In Figs. 5a-c we compare the results for  $\bar{\epsilon}_k$  for the (un)driven single transmon as a function of  $n_g$  at and away from freezing. The effect of variations in  $n_g$  can be understood as changing the level-spacing of the computational eigenstates leading to phase-errors. As anticipated, the weak  $n_g$  dependence of the low energy levels of the static transmon [panel (a)] becomes stronger when the transmon is driven, whether away from freezing [panel (b)] or at freezing [panel(c)].

Turning now to the driven fluxonium, we vary  $\varphi_{\text{ext}}$  between  $[0, 2\pi)$  instead of keeping it fixed at  $\varphi_{\text{ext}} = \pi$ . As noted in the introduction, variations in  $\varphi_{\text{ext}}$  change the level-spacing of the computational eigenstates leading to phase errors. Experimental protocols that provide robustness against any variations in the energy difference between the computational eigenstates as a function of  $\varphi_{\text{ext}}$  are thus highly desirable. As in our treatment of charge noise for transmons, instead of analyzing the effects of a fully time-dependent noise,  $\varphi_{\text{ext}}(t)$ , we make use of an adiabatic approximation below. We again assume that variations in  $\varphi_{\text{ext}}$  occur on a slower timescale com-

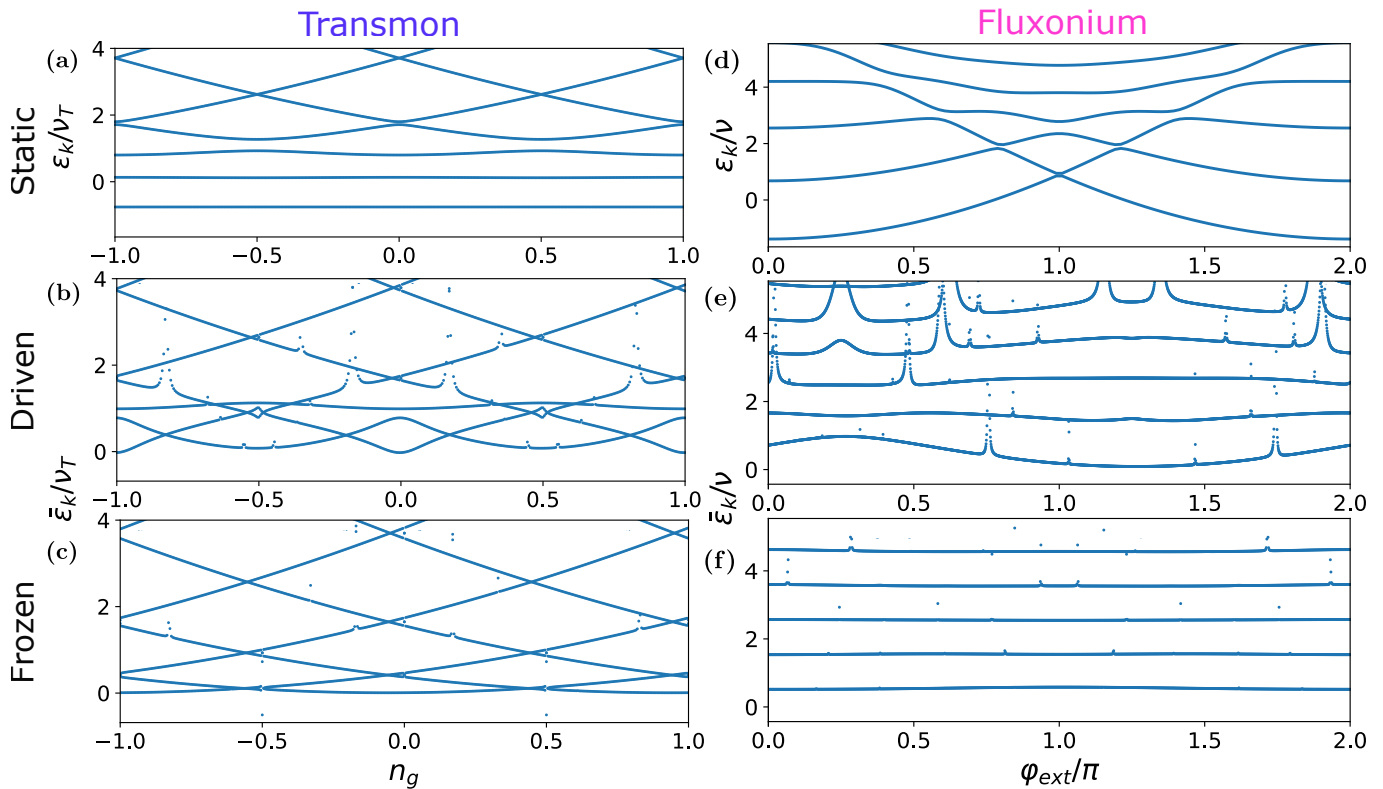


FIG. 5: We show the eigenenergies for the *static* (a) transmon, and (d) fluxonium, as a function of  $n_g$  and  $\varphi_{\text{ext}}$ , respectively and the period averaged quasi-energies,  $\bar{\varepsilon}_k$ , for a *driven* (b)-(c) transmon, and (e)-(f) fluxonium, as a function of  $n_g$  and  $\varphi_{\text{ext}}$ , respectively. The  $\bar{\varepsilon}_k$  are normalized by the transmon oscillator energy  $\nu_T/h = \sqrt{8E_J E_C}/h \approx 3.25$  GHz in panels (a)-(c), and by the fluxonium oscillator energy  $\nu$  (Eq. (13)) in panels (d)-(f). The drive frequency is  $\omega/\nu = 9.21$  for both. (b) and (e) are away from freezing, with  $\alpha = 1.5$ . (c) and (f) are at freezing, with  $\alpha = 2$ . Driven transmons at freezing appear somewhat less sensitive to variations in charge noise than transmons driven away from freezing. Nonetheless, both cases of driven transmon remain more sensitive to charge noise than static transmons. In contrast driven fluxonium away from freezing is less sensitive to variations in flux noise than static fluxonium (with the exception of resonances), and frozonium (f) is almost entirely independent to variations in flux noise.

pared to the relevant energy scales of our driven system, and treat  $\varphi_{\text{ext}}$  as a quenched variable.

The external flux shifts the Josephson and inductive terms relative to each other and thus can be chosen to only enter in the Josephson term [25] (see Eq. (6a)). As a result, at freezing points where the Josephson nonlinearities are strongly suppressed by a factor of  $1/\omega^2$ , we expect the system will have reduced dependence on  $\varphi_{\text{ext}}$  by the same factor. We thus anticipate that the phenomena of freezing will be robust against slow flux noise, and experience a lower tendency towards phase errors compared to the undriven system. In Figs. 5d-f, we compare the results for  $\bar{\varepsilon}_k$  for the (un-)driven fluxonium as a function of  $\varphi_{\text{ext}}$  at and away from freezing. There is a clear tendency for the different quasi-energy states to become largely insensitive to variations in  $\varphi_{\text{ext}}$  at freezing [panel (f)], compared to the undriven problem [panel (d)]. Away from freezing [panel (e)], while there are regions of  $\varphi_{\text{ext}}$  where the quasi-energies have minimal dependence on  $\varphi_{\text{ext}}$ , there are also isolated resonances, as discussed previously.

To summarize, we note that a clear benefit of frozo-

nium over driven transmons is the wider regime of protection against both flux and charge noise, in addition to the ability to tune the strength of induced nonlinearity away from freezing. Investigating this advantage in experiments in both driven transmons and frozonium in the vicinity of freezing points is an exciting future direction.

### III. Outlook

In this work we have analyzed the dynamical properties of a novel frozonium circuit, consisting of an inductively shunted Josephson junction under the effect of a Floquet drive. We have used a combination of numerical exact diagonalization and analytical calculations based on the Floquet-Magnus expansion for revealing the properties of frozonium over a wide range of drive amplitudes and frequencies, respectively. At special ratios of the drive amplitude and frequency, we have identified a set of isolated freezing points where the effective quantum dynamics of the frozonium is well-approximated by a simple harmonic

oscillator, supplemented by anharmonic nonlinear corrections that are suppressed in high powers of the drive frequency. Tuning away from these freezing points allows for additional continuous control of the degree of quantum nonlinearity. Treating the external flux-noise as a quenched variable in the adiabatic approximation, we have also demonstrated robust protection of the frozonium from decoherence. We find that the parametric dependence on magnetic flux is strongly suppressed at the freezing point, which suggests protection against dephasing from flux noise. We remark that result, using large classical flux fluctuations, connects to similar reductions in parametric flux dependence in the condition of large quantum phase fluctuations [51]. Additionally, we have clarified the phenomenology of the dynamically generated isolated resonances between the quasi-energy states separated by the drive frequency, which are undesirable from the point of view of quantum control.

We see two important practical applications of the dynamical control we have developed throughout this manuscript. Inspired by dynamical freezing and reduction in chaos in many-transmon systems [26], the first is to adapt this control to protect quantum information in many coupled frozonium from the spread of chaos over long times. At freezing points, the frozonium becomes approximately integrable. By tuning to these special points, a non-integrable, chaotic, coupled fluxonium system can be converted to be approximately integrable and non-chaotic. A possible impediment to this proposal in the case of transmon systems was due to the presence of noisy offset charge, which frozonium does not exhibit with respect to flux. Our theoretical analysis of the driven fluxonium (and previously the driven transmons [26]) has treated the problem as a closed and unitary quantum mechanical system. One interesting future direction would be to include the coupling of these driven many-body systems to an external bath, and analyze the robustness of the freezing phenomenology in the presence of weak dissipation.

Finally, we remark on a second potential application, namely bosonic quantum control. Over recent years, bosonic quantum computing has drawn significant interest due to its ability to implement several categories of error correcting codes and accomplish quantum simulation [52–55]. However, universal control schemes usually require coupling an ancilla qubit to the bosonic mode, which limits the performance of the bosonic mode because of the inferior coherence time of the ancilla [56].

The type of dynamical control over the fluxonium circuit described here therefore presents a new direction for bosonic control in which only a single dynamical mode is required. At freezing points we showed that driven fluxonium is well-approximated by a harmonic oscillator, and nonlinearity is introduced when tuning the drive parameters away from the freezing point. Therefore, with this kind of drive modulation, nonlinear bosonic control may be effected. We leave a targeted exploration of the power of this kind of control to a future study.

## Acknowledgments

We thank Michel Devoret for insightful discussions. KL acknowledges that this material is based upon work supported by the National Science Foundation Graduate Research Fellowship under Grant No. DGE – 2139899. HG is supported by a Wilkins postdoctoral fellowship at Cornell University. DC, RM and HG are supported in part by a New Frontier Grant awarded by the College of Arts and Sciences at Cornell University, and by a Sloan research fellowship to DC from the Alfred P. Sloan foundation.

### A. Additional Details: Floquet-Magnus Expansion

We supplement the results of Sec. II A with additional details here, for both the triangular and sine-wave drives, respectively. Let us note at the outset that the Floquet-Magnus expansion is a high-frequency perturbative expansion that equates a periodically driven *time-dependent* Hamiltonian into a *time-independent* one over one Floquet cycle and that the resulting series is not formally convergent. For quantum problems with an unbounded Hilbert space, the formalism is not strictly justified, but nevertheless provides a useful reference point for describing the exact numerical results. We also reiterate that the Floquet quasi-energies are only defined modulo  $\omega$ , leading to an energy “band-folding” for quasi-energies that exceed the drive frequency. The resonances between the different Floquet blocks (as discussed e.g. in Fig. 4) represent important quantum mechanical processes, that also controls the non-trivial thermalization dynamics of driven problems [49].

Returning now to the discussion in Sec. II A, let us compute the first two terms in the Floquet-Magnus expansion,

$$\mathcal{H}_{\text{eff}}^{(0)} = \frac{1}{T} \int_0^T dt \mathcal{H}_{\text{mov}}(t), \quad (\text{A1a})$$

$$\mathcal{H}_{\text{eff}}^{(1)} = \frac{1}{2iT} \int_0^T dt_1 \int_0^{t_1} dt_2 [\mathcal{H}_{\text{mov}}(t_1), \mathcal{H}_{\text{mov}}(t_2)], \quad (\text{A1b})$$

where  $\mathcal{H} = \mathcal{H}_{\text{mov}}$  (Eq. (6a)). Let  $F_m$  be the Fourier coefficients of  $e^{i\Theta(t)}$ ,

$$e^{i\Theta(t)} = \sum_m F_m e^{im\omega t}. \quad (\text{A2})$$

With this notation,

$$\mathcal{H}_{\text{eff}}^{(0)} = 4E_c \hat{n}^2 + \frac{E_L}{2} \hat{\varphi}^2 - \frac{E_J}{T} \int_0^T dt \cos(\hat{\varphi} - \Theta(t)) \quad (\text{A3a})$$

$$= 4E_c \hat{n}^2 + \frac{E_L}{2} \hat{\varphi}^2 - \frac{E_J}{2} (F_0^* e^{i\hat{\varphi}} + F_0 e^{-i\hat{\varphi}}). \quad (\text{A3b})$$



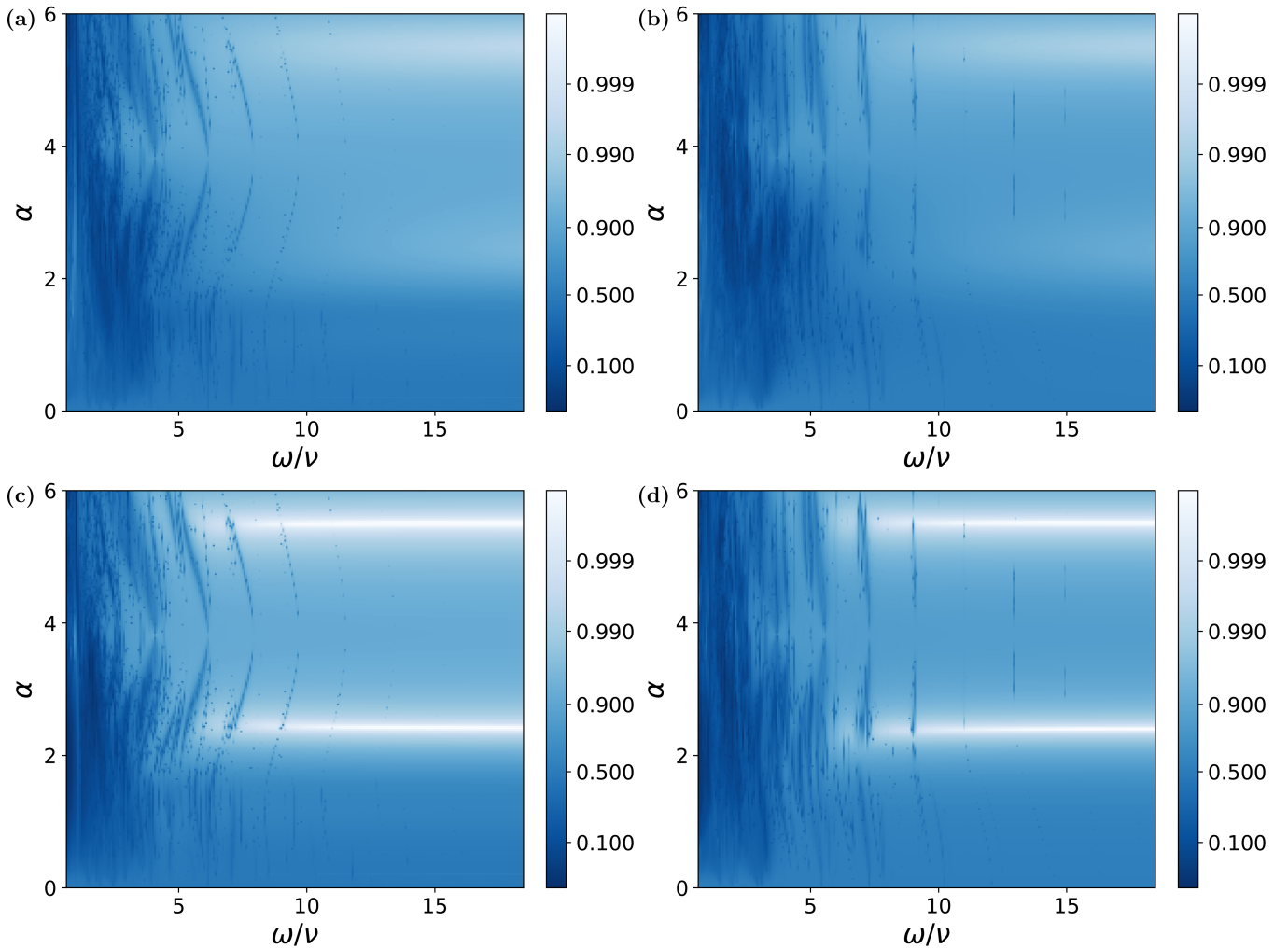


FIG. 6: The IPR (Eq. 12a) as a function of  $\alpha$  and  $\omega/\nu$  for a fluxonium driven via  $\Theta_{\sin}(t)$  (Eq. (7b)) with  $\varphi_{\text{ext}} = \pi$  time-averaged over  $N_F = 10,000$  cycles.  $|\Psi(0)\rangle$  is initialized to the (a) ground state, and (b) first excited state of  $H_{\text{quad}}$  in Eq. (6b). The horizontal bands of relatively high IPR  $> 0.9$  centered near  $\alpha = 2.4048, 5.5201$  are associated with the freezing region (see Eq. (A10)), but are weaker than the freezing regions for the triangular-wave drive (see Fig. 2). We use the same arctanh color scheme introduced in Fig. 2. The IPR is shown for  $|\Psi(0)\rangle$  initialized to the (c) ground state, and (d) first excited state of  $\mathcal{H}_{\text{eff}}|_{\alpha=\alpha_k^0}$  in Eq. (A11) (which includes the  $O(1/\omega)$  Floquet-Magnus correction). The value of IPR in the vicinity of the same freezing points increases significantly. All the Hamiltonian parameters are the same as in Fig 2.

To calculate  $\mathcal{H}_{\text{eff}}^{(1)}$ , we must integrate commutators of  $\mathcal{H}_{\text{mov}}$  at different times. The only time dependent component of  $\mathcal{H}_{\text{mov}}$  is the transformed Josephson energy term. Furthermore,

$$\left[ \frac{E_L}{2} \hat{\varphi}^2, E_J \cos(\hat{\varphi} - \Theta(t)) \right] = 0. \quad (\text{A4})$$

The commutators that appear in Eq. (A1) are thus independent of  $E_L$ . As a result, the first order term of the Magnus expansion for our fluxonium system are identical to the equivalent terms in the driven transmon system

[26], leading to

$$\mathcal{H}_{\text{eff}}^{(1)} = \frac{2}{\omega} E_c E_J [B(2\hat{n} + 1)e^{-i\hat{\varphi}} + \text{h.c.}] \quad (\text{A5a})$$

$$= \frac{2}{\omega} E_c E_J [\hat{n}(Be^{-i\hat{\varphi}} + B^*e^{i\hat{\varphi}}) + \text{h.c.}], \quad (\text{A5b})$$

where

$$B = \sum_{m \neq 0} \frac{F_m}{m}. \quad (\text{A6})$$

To simplify the expressions further, we need the explicit forms for  $F_m$ , which depend on the drive protocol.

## 1. Triangular wave drive

Let us consider the form of the drive introduced in Eq. (7a). The Fourier coefficients defined in Eq. (A2) are given by

$$F_m = -\frac{iA\omega \left(-1 + (-1)^m e^{\frac{i\pi A}{\omega}}\right)}{\pi(A^2 - m^2\omega^2)}. \quad (\text{A7})$$

Note that because  $F_m/m$  is an odd function of  $m$ , we have that  $B = 0$ . As a result,  $\mathcal{H}_{\text{eff}}^{(1)} = 0$ . Thus, from Eq. (A3b), at the leading order the effective Hamiltonian is given by

$$\mathcal{H}_{\text{eff}} = 4E_c \hat{n}^2 + \frac{E_L}{2} \hat{\varphi}^2 - \left(\frac{2}{\pi\alpha} \sin\left(\frac{\pi\alpha}{2}\right)\right) E_J \cos\left(\hat{\varphi} - \frac{\pi\alpha}{2}\right) + O\left(\frac{1}{\omega^2}\right). \quad (\text{A8})$$

As noted previously in the main text, the leading nonlinear correction involving the  $\cos \hat{\varphi}$  vanishes at particular values of  $\alpha = 2n$  for  $k \in \mathbb{Z}$  (Eq. (11a)).

## 2. Sine wave drive

For the sine wave drive in Eq. (7b),

$$F_m = J_m(\alpha), \quad \text{and} \quad (\text{A9a})$$

$$B = \frac{\pi}{2} \mathbf{H}_0(\alpha), \quad (\text{A9b})$$

where  $J_m$  are Bessel functions, and  $\mathbf{H}_0$  is the Struve function. The effective Hamiltonian then becomes,

$$\mathcal{H}_{\text{eff}} = 4E_c \hat{n}^2 + \frac{E_L}{2} \hat{\varphi}^2 - J_0(\alpha) E_J \cos \hat{\varphi} + \frac{2\pi}{\omega} \mathbf{H}_0(\alpha) E_c E_J (\hat{n} \cos \hat{\varphi} + \text{h.c.}) + O\left(\frac{1}{\omega^2}\right). \quad (\text{A10})$$

Note that at the zeros of  $J_0(\alpha)$ , the zeroth-order contribution from the Josephson term vanishes, leading to freezing. The nonlinear terms are suppressed in  $O(1/\omega)$ . The residual effective Hamiltonian at  $\alpha = \alpha_k^0$ , the  $k^{\text{th}}$  zero of  $J_0(\alpha)$ , is given by

$$\mathcal{H}_{\text{eff}} \Big|_{\alpha=\alpha_k^0} = 4E_c \hat{n}^2 + \frac{E_L}{2} \hat{\varphi}^2 + \frac{2\pi}{\omega} \mathbf{H}_0(\alpha_k^0) E_c E_J (\hat{n} \cos \hat{\varphi} + \text{h.c.}) + O\left(\frac{1}{\omega^2}\right) \quad (\text{A11})$$

As was discussed in the context of driven transmons [26], and will be shown in Appendix C, the  $O(1/\omega)$  correction weakens the quality of freezing, but has little effect on the level spacing of the driven system.

## B. Details of Numerical Computations

We discuss here additional details of the exact diagonalization (ED) computations. We have made use of the QuSpin PYTHON package [57, 58] to perform the ED analysis. We write the Hamiltonian in terms of bosonic raising and lowering operators  $b^\dagger, b$ ,

$$\hat{\varphi} = \left(\frac{2E_C}{E_L}\right)^{1/4} [b^\dagger + b], \quad (\text{B1})$$

$$\hat{n} = \frac{i}{2} \left(\frac{E_L}{2E_C}\right)^{1/4} [b^\dagger - b], \quad (\text{B2})$$

where  $[b, b^\dagger] = 1$ . This permits a number basis representation  $\{|n\rangle\}$  of our Hilbert space, which we truncate to keep only the lowest  $d_H$  states. Our operators written in terms of  $b^\dagger, b$  thus become  $d_H \times d_H$  dimensional matrices. We take  $d_H = 70$  throughout unless otherwise noted. In Fig. 7 we show that the time averaged Floquet eigenenergies converge well for this Hilbert space dimension in the presence of a drive.

Let us briefly note the method adopted for calculating the matrix elements of the nonlinear  $\cos(\hat{\varphi})$  term in the Hamiltonian. Rather than calculating it via a Taylor series expansion [26], we calculate it here exactly via a matrix cosine. Specifically, for a given Hermitian operator written as a matrix  $\hat{M}$  we note that,

$$\cos \hat{M} = \cos(\hat{U}^{-1} \hat{\Lambda} \hat{U}) = \hat{U}^{-1} \cos(\hat{\Lambda}) \hat{U}, \quad (\text{B3})$$

where  $\hat{U}$  is the transformation that diagonalizes the matrix, and  $\hat{\Lambda}$  is the resulting diagonal matrix consisting of the eigenvalues of  $\hat{M}$ . The diagonal matrix  $\cos(\hat{\Lambda})$  can be calculated via the element-wise application of cosine. By calculating matrix cosines exactly, we keep the important periodic structure of the cosine which is not captured by a Taylor expansion at any finite order.

To compute the time evolution of our system up to late times, we make use of the Floquet theorem. Specifically, in the presence of a time periodic Hamiltonian  $\mathcal{H}(t)$  with frequency  $\omega$  and period  $T = 2\pi/\omega$ , the time dependent eigenvectors of  $\mathcal{H}(t)$  can be written as  $|u_k(t)\rangle = e^{-i\varepsilon_k t} |\phi_k(t)\rangle$  for Floquet eigenvector  $|\phi_k(t)\rangle$  satisfying  $|\phi_k(t+T)\rangle = |\phi_k(t)\rangle$ , where the quasi-energy  $\varepsilon_k$  is defined up to modulo  $\omega$ . The Floquet eigenvectors  $\{\phi_k(0)\}$  can be calculated via diagonalizing the time ordered evolution operator over one period given by,

$$U(T, 0) = \left( \mathcal{T} \exp \left( - \int_0^T dt' i\mathcal{H}(t') \right) \right). \quad (\text{B4})$$

We can then determine the stroboscopic evolution of a state  $|\psi\rangle$  by projecting onto the Floquet eigenvector basis and evolving,

$$|\psi(t = nT)\rangle = \sum_k e^{-i\varepsilon_k nT} \langle \phi_k(0) | \psi(0) \rangle |\phi_k(0)\rangle, \quad (\text{B5})$$

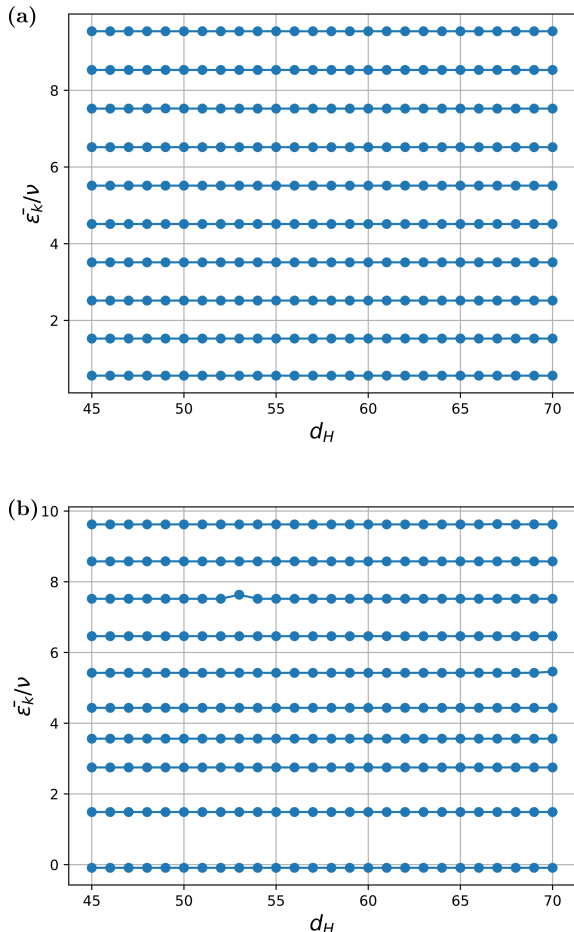


FIG. 7: The period averaged quasi-energies (a) at freezing,  $\alpha = 2$ , and (b) away from freezing,  $\alpha = 1$ , for various Hilbert space dimensions  $d_H$  up to a maximum of 70. The result is normalized by the fluxonium oscillator energy  $\nu$  (Eq. (13)). In both cases  $\omega/\nu = 12.31$ , and all other parameters are as in Fig. 2.

where  $n \in \mathbb{Z}$ . By using this method, we are able to make the computational time needed to determine  $|\psi(t = nT)\rangle$  fully independent of the value of  $nT$ . Finally, to compute the period-averaged quasienergies (Eq. (14a)), we discretize the integral into 50 equally spaced time slices, and average over the integrand computed at each of these slices.

For the numerical simulations of the transmon Hamiltonian, we work in the charge basis [59], where the full static part of the Hamiltonian is expressed as,

$$H_{\text{static}} = 4E_c(\hat{n} - n_g)^2 - \frac{E_J}{2} \sum_n \left( |n\rangle \langle n+1| + \text{h.c.} \right),$$

with  $\hat{n} = \sum_{n=-\infty}^{\infty} |n\rangle \langle n|$ . The Floquet drive is given by  $f(t)H_{\text{drive};\hat{n}}$ , where  $f(t)$  is given by Eq. (8a). For numerical simulations, we apply a cutoff at  $n = 10$ . We have verified that increasing the cutoff has a negligible

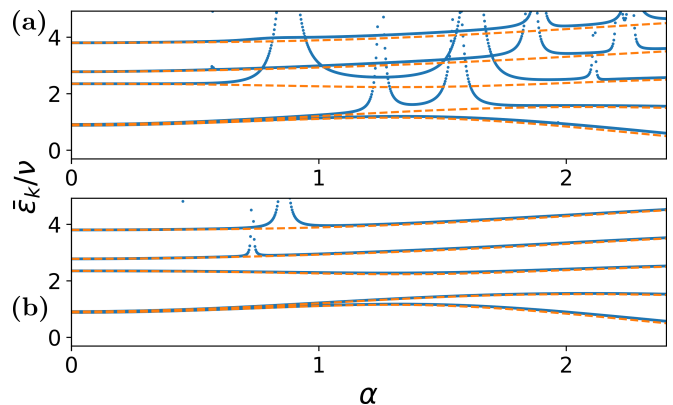


FIG. 8: The period averaged quasi-energies,  $\bar{\epsilon}_k$ , (Eq. (14a)) as a function of  $\alpha$  for a driven fluxonium at (a)  $\omega/\nu = 9.23$ , (b)  $\omega/\nu = 12.31$ . The result is normalized by the fluxonium oscillator energy  $\nu$  (Eq. (13)). All other parameters are the same as in Fig. 2. The right most edge of both plots corresponds to the first freezing point ( $\alpha = 2.4048$ ). Blue data points are obtained from numerical exact diagonalization. Orange dashed lines are obtained using the zeroth-order Floquet Magnus expansion (Eq. (10b)).

effect on the low-lying excitation spectrum in the regime of interest.

### C. Exact Diagonalization Results for Sine Drive

We now turn to analyzing the behavior of a single fluxonium driven with a sine wave drive. We will proceed in analogy to the analysis of the triangular wave drive in the main text, and observe the impact of a non-zero first-order in  $1/\omega$  term (as discussed in Eq. (A11)) on the resulting behavior near freezing. As before, we set  $d_H = 70$ , and choose  $\varphi_{\text{ext}} = \pi$  unless otherwise noted.

We start by studying quantitatively the extent to which the eigenstates for fluxonium driven by a sine drive overlap with the eigenstates of  $H_{\text{quad}}$  in Eq. (6b), and the oscillator described by  $\mathcal{H}_{\text{eff}}|_{\alpha=\alpha_k^0}$  described in Eq. (A11). For the former, we choose an eigenstate of  $H_{\text{quad}}$ , and for the latter we similarly choose an eigenstate of  $\mathcal{H}_{\text{eff}}|_{\alpha=\alpha_k^0}$ . In both cases, we time-evolve the initial state with the full driven Hamiltonian,  $\mathcal{H}_{\text{mov}}(t)$  in Eq. (6a), and compute the IPR at the end of  $N_F = 10,000$  cycles as in Eq. (12a). Importantly, note that the overlap of  $|\Psi(t)\rangle$  is to be evaluated with respect to  $|\Phi_i\rangle$ , which represents a complete eigenbasis associated with either  $H_{\text{quad}}$  in Eq. (6b), or  $\mathcal{H}_{\text{eff}}|_{\alpha=\alpha_k^0}$  in Eq. (A11).

In Fig. 6(a)-(b) we show the averaged IPR as a function of  $\alpha$  and  $\omega/\nu$ , with  $|\Psi(0)\rangle$  initialized to the ground and first excited states of  $H_{\text{quad}}$ , respectively. As expected, the bands of a large IPR  $> 0.9$  centered around the first two zeroes of  $J_0$  Bessel function,  $\alpha = 2.4048, 5.5201$ , are clearly visible. However, unlike for the triangle-wave drive, we find a lower value of the IPR near freezing (except for large  $\omega$ ). We conjecture that this is due to

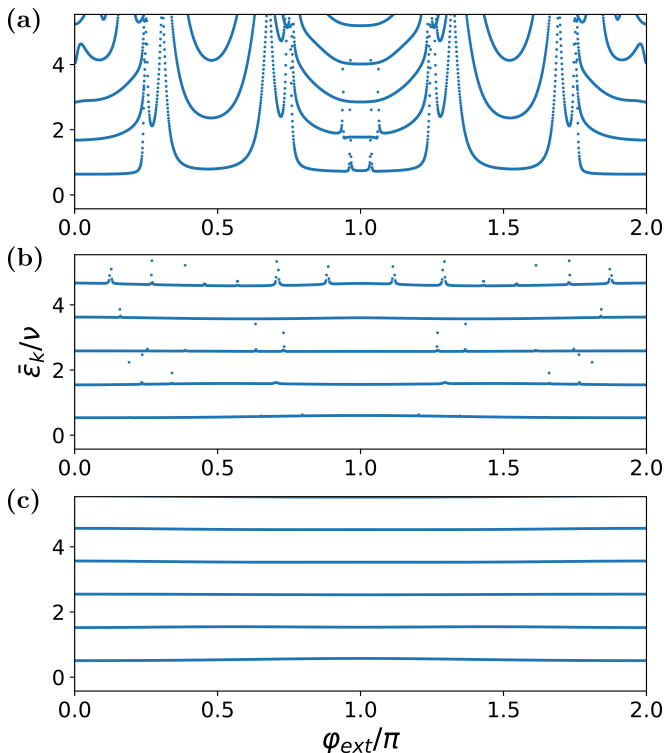


FIG. 9: We show the period averaged eigen-energies as a function of  $\varphi_{ext}$  for a single fluxonium driven by sine drive at the  $\alpha = 2.4048$  freezing point for (a)  $\omega/\nu = 6.15$ , (b)  $\omega/\nu = 9.23$ , and (c)  $\omega/\nu = 12.13$ . The result is normalized by the fluxonium oscillator energy  $\nu$  (Eq. (13)). All other parameters are the same as in Fig (2). With the exception of certain resonance points for low drive frequencies, the computational states of sine-wave driven fluxonium at freezing are almost entirely independent of external flux.

the non-vanishing first order correction in the Floquet-Magnus expansion for the sine-wave drive, which vanishes for the triangle-wave drive.

To test this hypothesis, in Fig. 6(c)-(d), we repeat the same analysis as above but for the the ground and first excited states of  $\mathcal{H}_{eff}|_{\alpha=\alpha_k^0}$  defined in Eq. (A11). Indeed, we find that the  $IPR \rightarrow 1$  is now significantly larger than before in the vicinity of the freezing points. Including the first order Floquet-Magnus correction term accounts for a better agreement with the effective dynamics of the driven problem.

While the existence of the first order term clearly has a measurable effect on the eigenstates themselves, it has no effect on the eigenenergies of the driven system. This is because the first-order Magnus correction (A1b) is explicitly gauge-dependent, i.e. it changes after shifting the time variable  $t \rightarrow t + \Delta t$ . According to the Floquet theorem, the Floquet quasienergy is independent of the gauge choice even though the eigenstates are gauge-dependent. In the following, we provide an alternative derivation using first-order perturbation theory. Let  $|\phi_k\rangle$  be the eigenstates of the zeroth order Magnus Hamiltonian  $\mathcal{H}_{eff}$  defined in Eq. (10b). The effect of the perturbative,  $O(1/\omega)$

Floquet-Magnus correction on the quasi-energy of these eigenstates is given by,

$$E_k^{(1)} = \langle \phi_k | \mathcal{H}_{eff}^{(1)} | \phi_k \rangle, \quad (C1a)$$

$$\mathcal{H}_{eff}^{(1)} = \frac{2\pi}{\omega} \mathbf{H}_0(\alpha) E_c E_J (\hat{n} \cos \hat{\varphi} + \text{h.c.}). \quad (C1b)$$

To analyze this term let us introduce the phase parity operator  $\Pi$  which acts on a wave function written in the phase representation as

$$\Pi |\psi(\varphi)\rangle = |\psi(-\varphi)\rangle. \quad (C2)$$

In analogy to the parity operator for the standard position and momentum representation,

$$\{\Pi, \hat{\varphi}\} = \{\Pi, \hat{n}\} = 0. \quad (C3)$$

Note that the Hamiltonian  $\mathcal{H}_{eff}$  is even in  $\hat{n}, \hat{\varphi}$ , so from our anticommutation relations  $[\Pi, \mathcal{H}_{eff}] = 0$ . This means that  $\mathcal{H}_{eff}$  and  $\Pi$  admit simultaneous eigenstates, so  $|\phi_k(\varphi)\rangle$  are all even or odd functions when written in the phase space representation.

Next note that  $\mathcal{H}_{eff}^{(1)}$  is an odd function of  $\hat{n}$ , but an even function of  $\hat{\varphi}$ , from our anticommutation relations  $\{\Pi, \mathcal{H}_{eff}^{(1)}\} = 0$ . As a result, acting  $\mathcal{H}_{eff}^{(1)}$  on an eigenstate of  $\Pi$  (and even or odd wavefunction) flips the parity of that state. Hence,  $\langle \phi_k |$  and  $\mathcal{H}_{eff}^{(1)} | \phi_k \rangle$  have opposite parities and thus have zero overlap. As such,  $E_k^{(1)} = 0$ . The first-order term of the Magnus expansion thus only contributes at  $O(1/\omega^2)$ , so the eigenenergies of the system driven by the sine drive should be equally well predicted by *only* the zeroth-order Magnus term as in the case of the triangle wave drive. This is in contrast to the *eigenstates* of the system which are renormalized at first order perturbation theory for the sine drive versus second order for the triangular-wave drive.

To see this numerically, in Fig. 8 we plot the lowest 5 period averaged quasi-energies (defined in Eq. (14a)) for a sine wave driven fluxonium, as a function of  $\alpha$  for two different drive frequencies,  $\omega$ . We also compute directly the same quantity based on the zeroth-order Floquet-Magnus expansion results (Eq. (10b)). We see that outside of resonance points, the zeroth order Magnus expansion predicts the energies of the states very well (similarly to the corresponding diagram for the triangle-wave drive, Fig 3).

Another consequence of this is that at freezing points, the period-averaged quasi-energies should be equivalent to that of  $H_{quad}$  up to  $O(1/\omega^2)$ . Thus, the driven Fluxonium with a sine-wave drive should be equally robust to flux noise as the triangle-wave drive. To analyze this numerically, in Fig. 9 we plot the period averaged quasi-energy of a single fluxonium qubit as a function of  $\varphi_{ext}$  at freezing for several values of  $\omega$ . Indeed, with the exception of the resonance points (whose number decreases with increasing  $\omega$ ), the low-lying computational states at freezing disperse minimally with the external flux.

**Author Contributions:** V. F. and D. C. determined the motivations for adding the inductive shunt; K. L., R. M., and H. G. performed the theoretical computations under supervision of D. C. with periodic input from S. R.

and V. F.; K. L. performed the frozonium numerical simulations, and R. M. performed the transmon numerical simulations; K. L. and D. C. wrote the manuscript with input from all authors.

- 
- [1] A. Blais, J. Gambetta, A. Wallraff, D. I. Schuster, S. M. Girvin, M. H. Devoret, and R. J. Schoelkopf, “Quantum-information processing with circuit quantum electrodynamics,” *Physical Review A—Atomic, Molecular, and Optical Physics* **75**, 032329 (2007).
- [2] J. Koch, T. M. Yu, J. Gambetta, A. A. Houck, D. I. Schuster, J. Majer, A. Blais, M. H. Devoret, S. M. Girvin, and R. J. Schoelkopf, “Charge-insensitive qubit design derived from the cooper pair box,” *Phys. Rev. A* **76**, 042319 (2007).
- [3] A. Blais, A. L. Grimsmo, S. M. Girvin, and A. Wallraff, “Circuit quantum electrodynamics,” *Rev. Mod. Phys.* **93**, 025005 (2021).
- [4] M. F. Bocko, A. M. Herr, and M. J. Feldman, “Prospects for quantum coherent computation using superconducting electronics,” *IEEE Transactions on Applied Superconductivity* **7**, 3638 (1997).
- [5] A. Shnirman, G. Schön, and Z. Hermon, “Quantum manipulations of small josephson junctions,” *Phys. Rev. Lett.* **79**, 2371 (1997).
- [6] Y. Nakamura, Y. A. Pashkin, and J. Tsai, “Coherent control of macroscopic quantum states in a single-cooper pair box,” *nature* **398**, 786 (1999).
- [7] C. Berke, E. Varvelis, S. Trebst, A. Altland, and D. P. DiVincenzo, “Transmon platform for quantum computing challenged by chaotic fluctuations,” *Nature communications* **13**, 2495 (2022).
- [8] S.-D. Börner, C. Berke, D. P. DiVincenzo, S. Trebst, and A. Altland, “Classical chaos in quantum computers,” *Phys. Rev. Res.* **6**, 033128 (2024).
- [9] D. Basilewitsch, S.-D. Börner, C. Berke, A. Altland, S. Trebst, and C. P. Koch, “Chaotic fluctuations in a universal set of transmon qubit gates,” (2024), arXiv:2311.14592 [quant-ph].
- [10] E. Varvelis and D. P. DiVincenzo, “Perturbative analysis of quasiperiodic patterning of transmon quantum computers: Enhancement of many-body localization,” *Phys. Rev. B* **109**, 144201 (2024).
- [11] A. Nico-Katz, N. Keenan, and J. Goold, “Can quantum computers do nothing?” (2024), arXiv:2406.16861 [quant-ph].
- [12] M. Silveri and T. Orell, “Many-qubit protection-operation dilemma from the perspective of many-body localization,” *nature communications* **13**, 5825 (2022).
- [13] F. Arute, K. Arya, R. Babbush, D. Bacon, J. C. Bardin, R. Barends, R. Biswas, S. Boixo, F. G. Brandao, D. A. Buell, *et al.*, “Quantum supremacy using a programmable superconducting processor,” *Nature* **574**, 505 (2019).
- [14] A. D. Córcoles, A. Kandala, A. Javadi-Abhari, D. T. McClure, A. W. Cross, K. Temme, P. D. Nation, M. Steffen, and J. M. Gambetta, “Challenges and opportunities of near-term quantum computing systems,” *Proceedings of the IEEE* **108**, 1338 (2020).
- [15] N. Didier, E. A. Sete, J. Combes, and M. P. da Silva, “ac Flux Sweet Spots in Parametrically Modulated Superconducting Qubits,” *Physical Review Applied* **12**, 054015 (2019).
- [16] A. Petrescu, M. Malekakhlagh, and H. E. Türeci, “Lifetime renormalization of driven weakly anharmonic superconducting qubits. II. The readout problem,” *Physical Review B* **101**, 134510 (2020).
- [17] P. S. Mundada, A. Gyenis, Z. Huang, J. Koch, and A. A. Houck, “Floquet-Engineered Enhancement of Coherence Times in a Driven Fluxonium Qubit,” *Physical Review Applied* **14**, 054033 (2020).
- [18] Z. Huang, P. S. Mundada, A. Gyenis, D. I. Schuster, A. A. Houck, and J. Koch, “Engineering Dynamical Sweet Spots to Protect Qubits from  $1/f$  Noise,” *Physical Review Applied* **15**, 034065 (2021).
- [19] J. Venkatraman, X. Xiao, R. G. Cortiñas, A. Eickbusch, and M. H. Devoret, “Static Effective Hamiltonian of a Rapidly Driven Nonlinear System,” *Physical Review Letters* **129**, 100601 (2022).
- [20] J. Cohen, A. Petrescu, R. Shillito, and A. Blais, “Reminiscence of Classical Chaos in Driven Transmons,” *PRX Quantum* **4**, 020312 (2023), publisher: American Physical Society.
- [21] A. Petrescu, C. Le Calonnec, C. Leroux, A. Di Paolo, P. Mundada, S. Sussman, A. Vrajitoarea, A. A. Houck, and A. Blais, “Accurate Methods for the Analysis of Strong-Drive Effects in Parametric Gates,” *Physical Review Applied* **19**, 044003 (2023).
- [22] X. Xiao, J. Venkatraman, R. G. Cortiñas, S. Chowdhury, and M. H. Devoret, “A diagrammatic method to compute the effective Hamiltonian of driven nonlinear oscillators,” (2024).
- [23] M. Thibodeau, A. Kou, and B. K. Clark, “The Floquet Fluxonium Molecule: Driving Down Dephasing in Coupled Superconducting Qubits,” *PRX Quantum* **5**, 040314 (2024).
- [24] Z. Wang and A. H. Safavi-Naeini, “Quantum control and noise protection of a floquet  $0-\pi$  qubit,” *Phys. Rev. A* **109**, 042607 (2024).
- [25] U. Vool and M. Devoret, “Introduction to quantum electromagnetic circuits,” *International Journal of Circuit Theory and Applications* **45**, 897 (2017).
- [26] R. Mukherjee, H. Guo, K. Lewellen, and D. Chowdhury, “Arresting quantum chaos dynamically in transmon arrays,” (2024), arXiv:2405.14935 [cond-mat.str-el].
- [27] J. Koch, T. M. Yu, J. Gambetta, A. A. Houck, D. I. Schuster, J. Majer, A. Blais, M. H. Devoret, S. M. Girvin, and R. J. Schoelkopf, “Charge-insensitive qubit design derived from the Cooper pair box,” *Physical Review A* **76**, 042319 (2007).
- [28] J. A. Schreier, A. A. Houck, J. Koch, D. I. Schuster, B. R. Johnson, J. M. Chow, J. M. Gambetta, J. Majer, L. Frunzio, M. H. Devoret, S. M. Girvin, and R. J. Schoelkopf, “Suppressing charge noise decoherence in superconducting charge qubits,” *Physical Review B* **77**, 180502 (2008).

- [29] M. Kjaergaard, M. E. Schwartz, J. Braumüller, P. Krantz, J. I.-J. Wang, S. Gustavsson, and W. D. Oliver, “Superconducting Qubits: Current State of Play,” *Annual Review of Condensed Matter Physics* **11**, 369 (2020).
- [30] N. P. de Leon, K. M. Itoh, D. Kim, K. K. Mehta, T. E. Northup, H. Paik, B. S. Palmer, N. Samarth, S. Sangtawesin, and D. W. Steuerman, “Materials challenges and opportunities for quantum computing hardware,” *Science* **372**, eabb2823 (2021).
- [31] A. Gyenis, A. Di Paolo, J. Koch, A. Blais, A. A. Houck, and D. I. Schuster, “Moving beyond the Transmon: Noise-Protected Superconducting Quantum Circuits,” *PRX Quantum* **2**, 030101 (2021).
- [32] V. E. Manucharyan, J. Koch, L. I. Glazman, and M. H. Devoret, “Fluxonium: Single Cooper-Pair Circuit Free of Charge Offsets,” *Science* **326**, 113 (2009).
- [33] A. Das, “Exotic freezing of response in a quantum many-body system,” *Phys. Rev. B* **82**, 172402 (2010).
- [34] B. Mukherjee, A. Sen, D. Sen, and K. Sengupta, “Dynamics of the vacuum state in a periodically driven rydberg chain,” *Phys. Rev. B* **102**, 075123 (2020).
- [35] A. Haldar, D. Sen, R. Moessner, and A. Das, “Dynamical freezing and scar points in strongly driven floquet matter: Resonance vs emergent conservation laws,” *Phys. Rev. X* **11**, 021008 (2021).
- [36] S. Aditya and D. Sen, “Dynamical localization and slow thermalization in a class of disorder-free periodically driven one-dimensional interacting systems,” *SciPost Phys. Core* **6**, 083 (2023).
- [37] H. Guo, R. Mukherjee, and D. Chowdhury, “Dynamical freezing in exactly solvable models of driven chaotic quantum dots,” (2024), arXiv:2405.01627 [cond-mat.str-el].
- [38] A. Haldar, A. Das, S. Chaudhuri, L. Staszewski, A. Wietek, F. Pollmann, R. Moessner, and A. Das, “Dynamical freezing in the thermodynamic limit: the strongly driven ensemble,” (2024), arXiv:2410.11050 [cond-mat.stat-mech].
- [39] J. Koch, V. Manucharyan, M. H. Devoret, and L. I. Glazman, “Charging Effects in the Inductively Shunted Josephson Junction,” *Physical Review Letters* **103**, 217004 (2009).
- [40] F. C. Wellstood, C. Urbina, and J. Clarke, “Low-frequency noise in dc superconducting quantum interference devices below 1 K,” *Applied Physics Letters* **50**, 772 (1987).
- [41] R. H. Koch, D. P. DiVincenzo, and J. Clarke, “Model for  $1/f$  flux noise in squids and qubits,” *Phys. Rev. Lett.* **98**, 267003 (2007).
- [42] S. M. Anton, J. S. Birenbaum, S. R. O’Kelley, V. Bolkhovskiy, D. A. Braje, G. Fitch, M. Neeley, G. C. Hilton, H.-M. Cho, K. D. Irwin, F. C. Wellstood, W. D. Oliver, A. Shnirman, and J. Clarke, “Magnetic Flux Noise in dc SQUIDS: Temperature and Geometry Dependence,” *Physical Review Letters* **110**, 147002 (2013).
- [43] S. Sendelbach, D. Hover, A. Kittel, M. Mück, J. M. Martinis, and R. McDermott, “Magnetism in SQUIDS at Millikelvin Temperatures,” *Physical Review Letters* **100**, 227006 (2008).
- [44] L. B. Nguyen, G. Koolstra, Y. Kim, A. Morvan, T. Chistolini, S. Singh, K. N. Nesterov, C. Jünger, L. Chen, Z. Pedramrazi, B. K. Mitchell, J. M. Kreikebaum, S. Puri, D. I. Santiago, and I. Siddiqi, “Blueprint for a high-performance fluxonium quantum processor,” *PRX Quantum* **3**, 037001 (2022).
- [45] L. B. Nguyen, Y.-H. Lin, A. Somoroff, R. Mencia, N. Grabon, and V. E. Manucharyan, “High-coherence fluxonium qubit,” *Phys. Rev. X* **9**, 041041 (2019).
- [46] R. Mukherjee, H. Guo, and D. Chowdhury, “Floquet-thermalization via instantons near dynamical freezing,” (2024), arXiv:2412.10498 [quant-ph].
- [47] R. Ketzmerick and W. Wustmann, “Statistical mechanics of floquet systems with regular and chaotic states,” *Phys. Rev. E* **82**, 021114 (2010).
- [48] J. Cohen, A. Petrescu, R. Shillito, and A. Blais, “Reminiscence of classical chaos in driven transmons,” *PRX Quantum* **4**, 020312 (2023).
- [49] N. O’Dea, F. Burnell, A. Chandran, and V. Khemani, “Prethermal stability of eigenstates under high frequency floquet driving,” *Phys. Rev. Lett.* **132**, 100401 (2024).
- [50] K. Serniak, S. Diamond, M. Hays, V. Fatemi, S. Shankar, L. Frunzio, R. Schoelkopf, and M. Devoret, “Direct Dispersive Monitoring of Charge Parity in Offset-Charge-Sensitive Transmons,” *Physical Review Applied* **12**, 014052 (2019).
- [51] I. V. Pechenezhskiy, R. A. Mencia, L. B. Nguyen, Y.-H. Lin, and V. E. Manucharyan, “The superconducting quasicharge qubit,” *Nature* **585**, 368 (2020).
- [52] W.-L. Ma, S. Puri, R. J. Schoelkopf, M. H. Devoret, S. M. Girvin, and L. Jiang, “Quantum control of bosonic modes with superconducting circuits,” *Science Bulletin* **66**, 1789 (2021).
- [53] Y. Liu, S. Singh, K. C. Smith, E. Crane, J. M. Martyn, A. Eickbusch, A. Schuckert, R. D. Li, J. Sinanan-Singh, M. B. Soley, T. Tsunoda, I. L. Chuang, N. Wiebe, and S. M. Girvin, “Hybrid Oscillator-Qubit Quantum Processors: Instruction Set Architectures, Abstract Machine Models, and Applications,” (2024).
- [54] W. Cai, Y. Ma, W. Wang, C.-L. Zou, and L. Sun, “Bosonic quantum error correction codes in superconducting quantum circuits,” *Fundamental Research* **1**, 50 (2021).
- [55] E. Crane, K. C. Smith, T. Tomesh, A. Eickbusch, J. M. Martyn, S. Kühn, L. Funcke, M. A. DeMarco, I. L. Chuang, N. Wiebe, A. Schuckert, and S. M. Girvin, “Hybrid oscillator-qubit quantum processors: Simulating fermions, bosons, and gauge fields,” (2024), arXiv:2409.03747 [quant-ph].
- [56] W.-L. Ma, S. Puri, R. J. Schoelkopf, M. H. Devoret, S. M. Girvin, and L. Jiang, “Quantum control of bosonic modes with superconducting circuits,” *Science Bulletin* **66**, 1789 (2021).
- [57] P. Weinberg and M. Bukov, “Quspin: a python package for dynamics and exact diagonalisation of quantum many body systems part i: spin chains,” *SciPost Physics* **2**, 003 (2017).
- [58] P. Weinberg and M. Bukov, “Quspin: a python package for dynamics and exact diagonalisation of quantum many body systems. part ii: bosons, fermions and higher spins,” *SciPost Physics* **7**, 020 (2019).
- [59] Q. Community, “Modeling transmon qubit cooper-pair box hamiltonian in the charge basis,” (2025).